In press at *Nature Geoscience*

The future life span of Earth's oxygenated atmosphere

Kazumi Ozaki[1,2*] and Christopher T. Reinhard[2,3,4]

[1]Department of Environmental Science, Toho University, Funabashi, Chiba 274-8510, Japan

[2]NASA Nexus for Exoplanet System Science (NExSS)

[3]School of Earth and Atmospheric Sciences, Georgia Institute of Technology, Atlanta, GA 30332, USA

[4]NASA Astrobiology Institute, Alternative Earths Team, Riverside, CA, USA

*Correspondence to: kazumi.ozaki@sci.toho-u.ac.jp

Abstract:

Earth's modern atmosphere is highly oxygenated and is a remotely detectable signal of its surface biosphere. However, the lifespan of oxygen-based biosignatures in Earth's atmosphere remains uncertain, particularly for the distant future. Here we use a combined biogeochemistry and climate model to examine the likely timescale of oxygen-rich atmospheric conditions on Earth. Using a stochastic approach, we find that the mean future lifespan of Earth's atmosphere, with oxygen levels more than 1% of the present atmospheric level, is 1.08 ± 0.14 billion years (1σ). The model projects that a deoxygenation of the atmosphere, with atmospheric O_2 dropping sharply to levels reminiscent of the Archaean Earth, will most probably be triggered before the inception of moist greenhouse conditions in Earth's climate system and before the extensive loss of surface water from the atmosphere. We find that future deoxygenation is an inevitable consequence of increasing solar fluxes, whereas its precise timing is modulated by the exchange flux of reducing power between the mantle and the ocean–atmosphere–crust system. Our results suggest that the planetary carbonate–silicate cycle will tend to lead to terminally CO_2-limited biospheres and rapid atmospheric deoxygenation, emphasizing the need for robust atmospheric biosignatures applicable to weakly oxygenated and anoxic exoplanet atmospheres and highlighting the potential importance of atmospheric organic haze during the terminal stages of planetary habitability.

Introduction

The field of exoplanet astronomy is on the verge of the first detailed characterization of the atmospheres of extrasolar planets, with heightened expectations for the potential detection of spectroscopic indicators of habitability, and possibly life, using the next generation of space and ground-based telescopes[1-3]. However, a robust framework for remote life detection requires a detailed understanding of the factors that lead to the emergence and long-term maintenance of atmospheric biosignatures, including a full understanding of potential atmospheric composition in the broader context of planetary biogeochemistry[4]. Although numerous potential atmospheric biosignatures have been proposed[5], molecular oxygen (O_2) and its photochemical by-product ozone (O_3) remain at the forefront of approaches toward remote life detection due to their strong absorption at visible and near-infrared wavelengths, the importance of biology in controlling their atmospheric abundances, and the potential for homogeneity in abundance throughout the atmospheric column[4,6]. As a result, significant effort has been directed toward understanding atmospheric oxygenation on habitable worlds and the factors that might lead to abiotic oxygen-rich atmospheres[7-9].

Earth's photosynthetic biosphere currently supports large gross fluxes of O_2 to the ocean-atmosphere system—roughly 9×10^{15} mol O_2 y^{-1} (ref.[10])—with the result that the modern atmosphere is 20.5% O_2 by volume. However, the presence of oxygenic phototrophs on its own may not be enough to maintain a strongly oxygenated atmosphere. Indeed, it is generally thought that the abundance of O_2 in Earth's atmosphere has been well below that of today for most of Earth's history[11], and that the modern atmospheric O_2 abundance developed only after the emergence of land plants[12,13], which have evolved to accelerate the geochemical cycles of bioessential elements (most importantly phosphorus) in Earth surface environments[14,15]. Thus, charting the history of planetary oxygenation after the evolution of oxygenic photosynthesis requires an understanding of how biospheric productivity (and the subsequent burial of reduced materials into sediments) changes in response to evolving environmental conditions.

Previous work on the future lifespan of Earth's biosphere has focused principally on the links between secular changes in solar luminosity, the stability of the carbonate-silicate geochemical cycle, and the loss of surface water to space[16-20]. One robust result that emerges from this theoretical framework is a continuous decrease in the abundance of atmospheric CO_2 through time, as steadily increasing solar luminosity inexorably drives down the abundance of atmospheric CO_2 that is required to balance rates of crustal weathering with volcanic CO_2 output[16,17,21]. However, a number of models suggest that in spite of this thermal buffering mechanism Earth will enter the "moist greenhouse" climate state at some point within the next ~2 billion

years (Ga)—a regime in which elevated atmospheric temperatures allow Earth's stratosphere to become moist, leading to permanent water loss from Earth's surface[16-19,22,23]. In addition, this drawdown of atmospheric CO_2 may result in a fundamental shift to a photosynthetic biosphere that is CO_2-limited—for instance, some models predict that terrestrial C_3 plants will cease to be viable at Earth's surface less than ~500 Myr into Earth's future[16]. If true, this might place a long-term physical limit on the ability of photosynthetic biospheres to maintain high levels of atmospheric oxygen, giving rise to a fundamental trade-off between long-term stellar evolution, the geologic carbon cycle, and the intrinsic timescale of atmospheric oxygenation.

Here, we examine the future lifespan of Earth's oxygenated atmosphere using an Earth system model of biogeochemistry and climate (**Fig. 1**; see Methods). Assessing the lifespan of Earth's oxygenated atmosphere requires quantitative models that include a complete treatment of oxygen-related biogeochemical processes at the planetary surface over geologic time, as well as mechanistic linkages between surface environments and the planetary interior. Our model builds upon previous similar Earth system models[12] that track the coupled carbon, oxygen, phosphorus, and sulphur cycles in the exogenic (i.e., atmosphere, ocean, and crust) system (**Fig. 1**). However, we extend this framework by incorporating a global biogeochemical methane (CH_4) cycle, including a range of key biological metabolisms, parameterized atmospheric photochemistry within the O_2-O_3-CH_4 system[24,25], and the radiative impact of CH_4 on global energy balance[26].

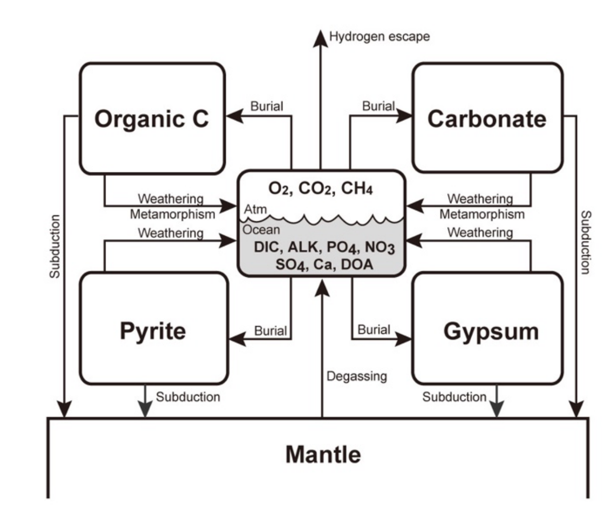


Fig. 1. Schematic model structure. Boxes denote reservoirs, whereas arrows denote flux terms. The model tracks the major reservoirs and transfer fluxes within the surface carbon (C), sulphur (S), oxygen (O), and phosphorus (P) cycles, along with a comprehensive treatment of ocean biogeochemistry, and long-term transfers between the crust-ocean-atmosphere system and the mantle. DOA = degree of anoxia.

Our model is also the first of its type to explicitly evaluate redox exchange between the crust and mantle, allowing a comprehensive evaluation of the planetary processes controlling atmospheric O_2 levels over geologic time. The model is designed to capture the major components of Earth system biogeochemistry and climate, but is abstracted enough to allow for large model ensembles that can be run for billions of years of model time. We employ a stochastic approach in which we draw randomly from a wide range of potential values for parameters controlling the major geophysical boundary conditions of the model,

including variability (cycle and amplitude) in outgassing rates and erosional forcing (see Methods and Extended Data Figs. 1-3), and initialize the model at 600 Ma. We then repeatedly run the model forward in time until the present day (n =~400,000), and subsample model runs (n = 4,787) that roughly reproduce modern atmospheric composition (pO_2 = 21±1% and pCO_2 = 300±150 ppmv), global average surface temperature (288±2K), and seawater sulphate (SO_4^{2-}) levels (SO_4^{2-} = 25±15 mM). The simulations from this subsampled ensemble are then run forward in time in order to estimate the future lifespan of Earth's oxygenated atmosphere.

Solar brightening promotes atmospheric deoxygenation

Our default analysis (**Fig. 2** and Extended Data Figs. 4-8) indicates that atmospheric O_2 levels will decrease substantially in Earth's long-term future (**Fig. 2a**). Whilst the magnitude and timing of this trajectory show a certain degree of uncertainty, the model-projected decrease in atmospheric O_2 abundance is robust and suggests that the future lifespan of Earth's oxygenated atmosphere will be less than 1.5 Gyr. Specifically, when we define the future lifespan as the period within which atmospheric O_2 remains above a given threshold value, the lifespan of atmospheric O_2 levels greater than 1% of the present atmospheric level (PAL)—$\tau_{1\%PAL}$—is estimated at 1.08±0.14 Gyr (1σ). Increasing the threshold value to 10% PAL results in a broadly similar lifespan of $\tau_{10\%PAL}$ = 1.05±0.16 Gyr (1σ), a consequence of the extremely short timescale over which atmospheric deoxygenation occurs. Several factors are responsible for the secular decrease in atmospheric O_2 (see Supplementary Information), most notably increasing surface temperatures and atmospheric CO_2 starvation of the terrestrial photosynthetic biosphere driven by solar brightening (**Fig. 2c** and Extended Data Figs. 4-7). Indeed, when we repeat our analysis with a constant solar luminosity we find that no secular O_2 trend remains (**Fig. 2a** and Extended Data Fig. 4). As the geologic drivers of the decreasing CO_2 trend (solar brightening and mantle cooling) are largely undisputed, the first-order features of our projected atmospheric O_2 trajectory should be robust.

Our model further predicts that CO_2 limitation of Earth's photosynthetic biosphere should ultimately lead to photochemical destabilization of Earth's oxygenated atmosphere and an abrupt shift in atmospheric O_2 abundance to very low values (**Fig. 2a**). Indeed, our model projects an atmospheric composition for Earth's long-term future that is similar in many respects to that of the Archaean Earth prior to the so-called 'Great Oxidation Event'[27]. In particular, atmospheric O_2 drops to values that are many orders of magnitude below that of the modern atmosphere ($<10^{-6}$ PAL), while the atmospheric abundance of CH_4 increases sharply (Fig. 2b). However, a critical difference from the Archaean Earth

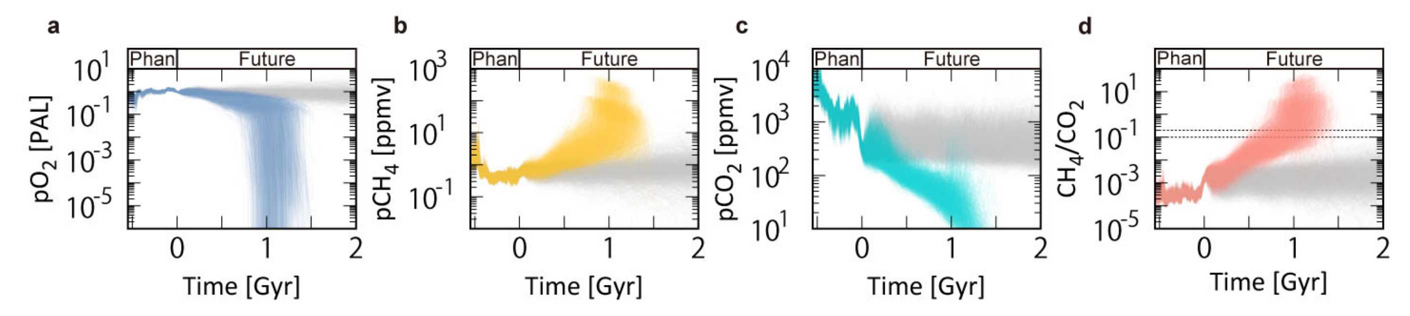


Fig. 2. Evolution of atmospheric chemistry in our stochastic analysis. Blue, orange, and green lines represent atmospheric O_2 (**a**), CH_4 (**b**), and CO_2 (**c**) concentrations obtained from our default model ensemble (*n* = 4,787), along with the predicted atmospheric CH_4/CO_2 ratios (red lines in **d**). Horizontal dotted lines in **d** represent a range of values between 0.1-0.2, broadly considered to define a threshold for the inception of organic haze formation[28-30]. All panels also show results obtained by running the same model ensemble with constant solar luminosity (grey lines). Phan = Phanerozoic.

system is the prediction of much lower atmospheric CO_2 levels in Earth's long-term future (**Fig. 2c**) and thus the potential for greatly elevated CH_4/CO_2 ratios (**Fig. 2d**). Such elevated CH_4/CO_2 ratios are generally predicted to result in the formation of 'organic haze' in the atmosphere[28-30], with potentially important impacts on climate, atmospheric redox chemistry, and remote life detection. Our results thus suggest that organic haze will be a critical component of Earth's long-term climate stability into the far future, as well as a potentially promising atmospheric biosignature on Earth-like worlds round late main-sequence stars such as the exoplanet candidate Kepler-452b (orbiting a G2 star with an age of ~6±2 Gyr and receiving ~10% more insolation than Earth receives from the Sun today)[31,32].

Controls on the timing of atmospheric deoxygenation

Our default analysis provides the first systematic estimate of the potential lifetime of Earth's oxygenated atmosphere into the far future. However, it is important to note that our default model ensemble includes a robust terrestrial biosphere, which may not be a universal feature of habitable Earth-like planets. To examine the impact of the terrestrial biosphere on the longevity of the O_2/O_3-based biosignatures, we performed an additional ensemble analysis in which we remove the terrestrial biosphere from our default successful runs (Extended Data Figs. 4 and 10). As expected, the absence of land plants results in somewhat lower atmospheric O_2 levels throughout the course of planetary evolution relative to our default analysis. However, we find that the future lifespan of Earth's remotely-detectable oxygenated atmosphere is similar to that of our default analysis (e.g., $\tau_{1\%PAL}$ = $1.04^{+0.17}_{-0.16}$ Gyr; cf. 1.08±0.14 Gyr for the default simulations) (**Fig. 3a**). This is an important result, as it strongly suggests that the presence or absence of terrestrial biosphere exerts a secondary control on the timescale of the planetary deoxygenation and long-term atmospheric redox state. Although it is difficult

to explicitly model uncertainties associated with biological evolution and adaptation in photosynthetic lineages, our statistical approach explores a wide range of parameter space for key biological response functions (see Methods and Extended Data Figs. 1-3), with results suggesting that uncertainty in the parameters governing the response of the biosphere plays a secondary role in controlling the future lifespan of oxygenated atmospheric conditions on Earth (Extended Data Fig. 9).

Our analysis also delineates an important relationship between the future lifespan of oxygenated atmospheric conditions and the long-term average flux of reducing power from the mantle to the surface system, $\Phi_{1\%}(\mathrm{Red})$ (**Fig. 3b**). In particular, our model suggests that larger $\Phi_{1\%}(\mathrm{Red})$ values tend to yield shorter oxygenated lifespans. Improvements in quantitative estimates of subduction and mantle degassing over time would reduce uncertainty in estimates of the future lifespan of Earth's oxygenated atmosphere, and will be critical for extending our model framework to very different tectonic regimes. In addition, our analysis suggests that oceanic redox chemistry—which ultimately controls oceanic P levels and the redox state and subduction fluxes of major C, S, and Fe species in the exogenic system—would be critical for the long-term trajectory of atmospheric redox state on habitable Earth-like planets (**Fig. 3b** and Extended Data Fig. 4). The lifespans of oxygen-rich atmospheric states on Earth-like planets are thus likely to be modulated by mantle redox state, rates of surface-interior exchange, and their evolution through time.

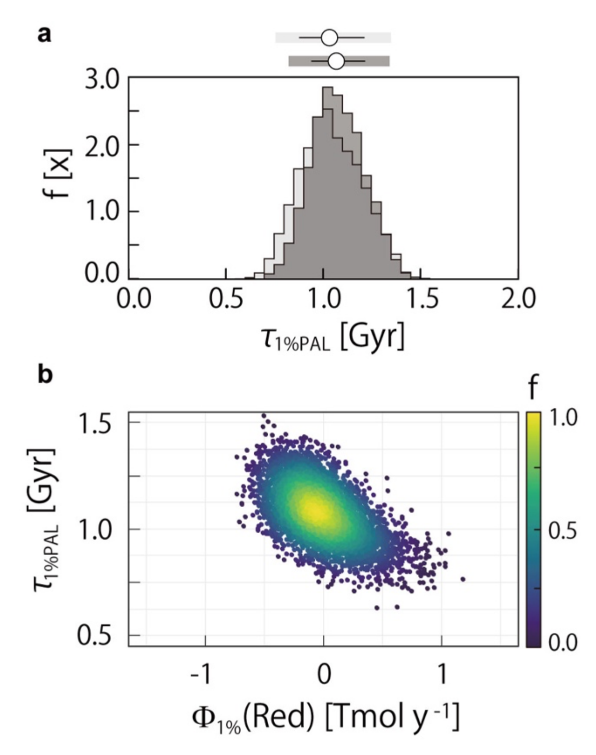


Fig. 3. The future lifespan of Earth's oxygenated atmosphere. (**a**) Posterior probability density distributions from our default analysis for Earth systems with (dark grey) and without (light grey) a terrestrial biosphere. Open circles denote median values, while the error bar and shaded region denote 1σ and 95% credible intervals, respectively. (**b**) The future lifespan of Earth's oxygenated atmosphere ($\tau_{1\%PAL}$) as a function of the average net input flux of reducing power from the mantle to the surface system. Positive values indicate net input of reducing power from the mantle to the surface system (see Methods). Each point is a single model run, while the colour scale denotes data density within the overall model ensemble. We note that there are a small number of scenarios in which atmospheric O_2 levels do not reach 1%PAL during the simulation, but such scenarios are very rare (~4%) and would rely on a fortuitous combination of parameter values.

It is important to note that there are multiple biogeochemical and climate processes that are not considered in our model that may play a role in constraining the future lifespan of

Earth's biosphere and the timing/mode of transition to more reducing atmospheric conditions. In particular, "reverse weathering" (the formation of authigenic silicates in marine sediments, resulting in net CO_2 release to the ocean-atmosphere system)[33] could potentially extend the lifespan of oxygenated atmospheric conditions under certain scenarios by prolonging the timescale over which atmospheric CO_2 is above the levels expected to result in CO_2 limitation of the photosynthetic biosphere[34]. On the other hand, this process would commensurately elevate global temperature in the face of increasing solar luminosity, with a corresponding potential for limitation of biospheric O_2 fluxes (Extended Data Fig. 1). The net effect on the future lifespan of Earth's oxygenated atmosphere is uncertain, but is likely of secondary importance to the overall trend presented here (see also Extended Data Fig. 5 for the sensitivity to terrestrial weatherability). In addition, we hypothesize that haze-induced climate cooling[28] could potentially act as a brake on the overall magnitude of atmospheric deoxygenation, or result in the inception of oxygenation/deoxygenation cycles during Earth's terminal habitability. Both of these topics represent important areas of future research.

Implications for the search for life on exoplanets

Our results also have important implications for the search for life on Earth-like planets beyond our solar system (e.g., habitable planets with abundant liquid water at the surface, exposed silicate crust, and a biosphere with oxygenic photosynthesis). From the perspective of planetary evolution, our results imply that atmospheric oxygenation is not a permanent condition on habitable worlds hosting oxygenic photosynthesis, and that only a fraction of Earth's history will be characterized by robustly detectable levels of atmospheric O_2 (**Fig. 4**). For example, it is estimated that a G-dwarf stellar flux ~20% greater than that of the present Sun (S/S_0 ~ 1.2) is required to achieve a water loss timescale of ~1 Gyr in the moist greenhouse regime[35]. Assuming it will take ~2 Gyr to achieve S/S_0 ~ 1.2 (ref.[36]), together with the assumption of surface liquid water by 4.4 Ga[37], yields an estimated habitable lifetime on Earth of ~7.4 Gyr. Our results indicate that direct detection of O_2 at visible wavelengths would be challenging for all but ~1.5-2.0 Gyr of this history — or roughly 20-30% of Earth's lifetime as a habitable world[38]. On the other hand, observations of O_3 at UV wavelengths[39] could potentially significantly extend this observability timescale (Fig. 4). In any case, our model suggests that a fundamental feature of the carbonate-silicate cycle, considered central to the long-term maintenance of habitable climate conditions on terrestrial planets, may ultimately act to drive atmospheric composition toward an anoxic, hazy state similar to that of the Archaean Earth but with much lower atmospheric CO_2. These predictions emphasize the need to better understand the factors regulating redox

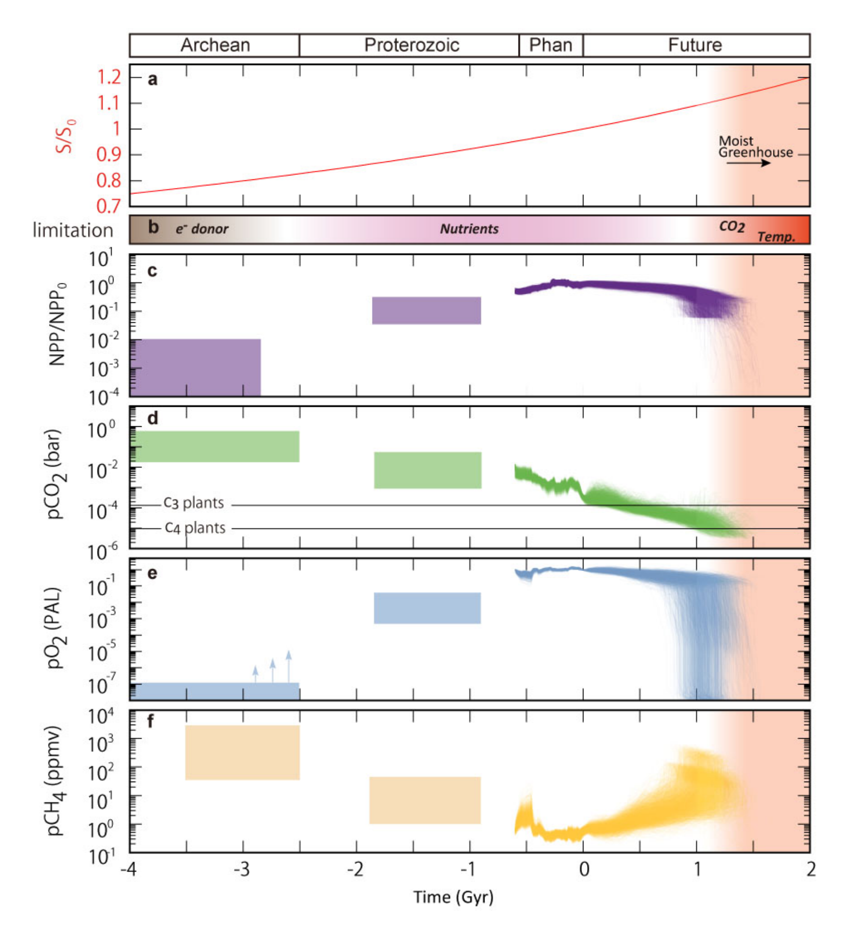


Fig. 4. The coupled evolution of Earth's biosphere and atmospheric chemistry. (a) Solar constant (normalized by modern value)[16]. (b) Limiting factor for biospheric activity. (c) Global net primary production (normalized to the modern value)[45,46]. (d) Atmospheric CO_2 level (in bar) [47]. (e) Atmospheric O_2 level (relative to the present atmospheric level, PAL)[11]. (f) Atmospheric CH_4 level (in parts per million by volume, ppmv). The atmospheric CH_4 level and global NPP during the mid-Archean and mid-Proterozoic are based on ref.[45,46]. The historical trajectory of biospheric productivity suggests that despite evolving limitations on overall biospheric fertility the biosphere has significantly altered the chemical composition of the atmosphere[45,46,48-50]. Our model, however, demonstrates that Earth's modern biosphere reaches the turning point at which the activity level of the biosphere begins to decline (see also Extended Data Figs. 4-7), and that the availability of inorganic carbon in combination with increased surface temperature will become the major limiting factor for global ecosystems. The orange-red shaded region denotes the inception of the moist greenhouse climate regime.

balance between the planetary interior and surface environments[40-44], and provide additional motivation for implementing a wide wavelength range in future exoplanet characterization missions as a contingency against "false negatives" for remote life detection[3,38].

In sum, our stochastic analysis suggests that the eventual deoxygenation of Earth's atmosphere is a robust outcome of increasing solar luminosity, irrespective of large uncertainties in geophysical/biological boundary conditions, and that the collapse of Earth's oxygenated atmosphere is likely to occur before the inception of moist greenhouse conditions in Earth's climate system although its precise timing is modulated by net input flux of reducing power from the mantle to Earth's surface system. In addition, our model projections of atmospheric chemistry implicate organic haze as a critical factor in regulating Earth's long-term future climate. Evaluating these factors using more sophisticated biogeochemistry and climate models is an important task for future research. Nevertheless, our analysis clearly identifies the first-order response of atmospheric O_2 to declining CO_2 and biospheric productivity, opening a new perspective on the future evolution of Earth's climate and atmospheric redox chemistry.

References

1 Fujii, Y. et al. Exoplanet Biosignatures: Observational Prospects. Astrobiology 18, 739-778, doi:10.1089/ast.2017.1733 (2018).

2 National Academies of Sciences, E. & Medicine. An Astrobiology Strategy for the Search for Life in the Universe. (The National Academies Press, 2019).

3 The LUVOIR Team. The LUVOIR Mission Concept Study Final Report. arXiv e-prints, arXiv:1912.06219 (2019). <https://ui.adsabs.harvard.edu/abs/2019arXiv191206219T>.

4 Meadows, V. S. et al. Exoplanet Biosignatures: Understanding Oxygen as a Biosignature in the Context of Its Environment. Astrobiology 18, 630-662, doi:10.1089/ast.2017.1727 (2018).

5 Schwieterman, E. W. et al. Exoplanet Biosignatures: A Review of Remotely Detectable Signs of Life. Astrobiology 18, 663-708, doi:10.1089/ast.2017.1729 (2018).

6 Meadows, V. Reflections on O_2 as a Biosignature in Exoplanetary Atmospheres. Astrobiology 17, 1022-1052, doi:10.1089/ast.2016.1578 (2017).

7 Wordsworth, R. & Pierrehumbert, R. Abiotic Oxygen-dominated Atmospheres on Terrestrial Habitable Zone Planets. The Astrophysical Journal Letters 785, L20 (2014).

8 Gao, P., Hu, R., Robinson, T. D., Li, C. & Yung, Y. L. Stability of CO_2 Atmospheres on Desiccated M Dwarf Exoplanets. Astrophys. J. 806, 249 (2015).

9 Luger, R. & Barnes, R. Extreme Water Loss and Abiotic O_2 Buildup on Planets Throughout the Habitable Zones of M Dwarfs. Astrobiology 15, 119-143, doi:10.1089/ast.2014.1231 (2015).

10 Prentice, I. C. et al. in Climate Change 2001: the Scientific Basis (eds J. T. Houghton et al.) Ch. 183-238, (Cambridge University Press, 2001).

11 Lyons, T. W., Reinhard, C. T. & Planavsky, N. J. The rise of oxygen in Earth's early ocean and atmosphere. Nature 506, 307-315, doi:10.1038/nature13068 (2014).

12 Lenton, T. M. et al. Earliest land plants created modern levels of atmospheric oxygen. Proc. Natl Acad. Sci. USA 113, 9704-9709, doi:10.1073/pnas.1604787113 (2016).

13 Krause, A. J. et al. Stepwise oxygenation of the Paleozoic atmosphere. Nature Commun. 9, 4081, doi:10.1038/s41467-018-06383-y (2018).

14 Lenton, T. M. Gaia and natural selection. Nature 394, 439-447, doi:10.1038/28792 (1998).

15 Lenton, T. M., Crouch, M., Johnson, M., Pires, N. & Dolan, L. First plants cooled the Ordovician. Nature Geosci 5, 86-89,

doi:https://doi.org/10.1038/ngeo1390 (2012).

16 Caldeira, K. & Kasting, J. F. The life span of the biosphere revisited. Nature 360, 721-723 (1992).

17 Lovelock, J. E. & Whitfield, M. Life span of the biosphere. Nature 296, 561-563 (1982).

18 Franck, S., Bounama, C. & von Bloh, W. Causes and timing of future biosphere extinctions. Biogeosciences 3, 85-92, doi:10.5194/bg-3-85-2006 (2006).

19 Franck, S., Kossacki, K. J., Von Bloth, W. & Bounama, C. Long-term evolution of the global carbon cycle: historic minimum of global surface temperature at presen. Tellus B 54 (2002).

20 O'Malley-James, J. T., Greaves, J. S., Raven, J. A. & Cockell, C. S. Swansong biospheres: refuges for life and novel microbial biospheres on terrestrial planets near the end of their habitable lifetimes. International Journal of Astrobiology 12, 99-112, doi:10.1017/s147355041200047x (2013).

21 Walker, J. C. G., Hays, P. B. & Kasting, J. F. A negative feedback mechanism for the long-term stabilization of Earth's surface temperature. J. Geophys. Res. 86, 9776-9782, doi:10.1029/JC086iC10p09776 (1981).

22 Kasting, J. F. Runaway and moist greenhouse atmospheres and the evolution of Earth and Venus. Icarus 74, 472-494, doi:https://doi.org/10.1016/0019-1035(88)90116-9 (1988).

23 Leconte, J., Forget, F., Charnay, B., Wordsworth, R. & Pottier, A. Increased insolation threshold for runaway greenhouse processes on Earth-like planets. Nature 504, 268-271, doi:10.1038/nature12827 (2013).

24 Claire, M. W., Catling, D. C. & Zahnle, K. J. Biogeochemical modelling of the rise in atmospheric oxygen. Geobiology 4, 239-269, doi:10.1111/j.1472-4669.2006.00084.x (2006).

25 Reinhard, C. T. et al. Oceanic and atmospheric methane cycling in the cGENIE Earth system model. Geosci. Model Dev. Discuss. 2020, 1-45, doi:10.5194/gmd-2020-32 (2020).

26 Byrne, B. & Goldblatt, C. Radiative forcing at high concentrations of well-mixed greenhouse gases. Geophys. Res. Lett. 41, 152-160, doi:10.1002/2013gl058456 (2014).

27 Holland, H. D. Volcanic gases, black smokers, and the great oxidation event. Geochim. Cosmochim. Acta 66, 3811-3826, doi:http://dx.doi.org/10.1016/S0016-7037(02)00950-X (2002).

28 Arney, G. et al. The Pale Orange Dot: The Spectrum and Habitability of Hazy Archean Earth. Astrobiology 16, 873-899, doi:10.1089/ast.2015.1422 (2016).

29 Haqq-Misra, J. D., Domagal-Goldman, S. D., Kasting, P. J. & Kasting, J. F. A Revised, Hazy Methane Greenhouse for the Archean Earth. Astrobiology 8, 1127-1137, doi:10.1089/ast.2007.0197 (2008).

30 Trainer, M. G. et al. Haze Aerosols in the Atmosphere of Early Earth: Manna from Heaven. Astrobiology 4, 409-419, doi:10.1089/ast.2004.4.409 (2004).

31 Jenkins, J. M. et al. Discovery and validation of Kepler-452b: A 1.6R⊕ super Earth exoplanet in the habitable zone of a G2 star. The Astronomical Journal 150, 56, doi:10.1088/0004-6256/150/2/56 (2015).

32 Mullally, F., Thompson, S. E., Coughlin, J. L., Burke, C. J. & Rowe, J. F. Kepler's Earth-like Planets Should Not Be Confirmed without Independent Detection: The Case of Kepler-452b. The Astronomical Journal 155, 210, doi:10.3847/1538-3881/aabae3 (2018).

33 Mackenzie, F. T. & Kump, L. R. Reverse Weathering, Clay Mineral Formation, and Oceanic Element Cycles. Science 270, 586-586, doi:10.1126/science.270.5236.586 (1995).

34 Isson, T. T. & Planavsky, N. J. Reverse weathering as a long-term stabilizer of marine pH and planetary climate. Nature 560, 471-475, doi:10.1038/s41586-018-0408-4 (2018).

35 Wolf, E. T., Shields, A. L., Kopparapu, R. K., Haqq-Misra, J. & Toon, O. B. Constraints on Climate and Habitability for Earth-like Exoplanets Determined from a General Circulation Model. Astrophys. J. 837, 107, doi:10.3847/1538-4357/aa5ffc (2017).

36 Gough, D. O. Solar interior structure and luminosity variations. Sol. Phys. 74, 21-34, doi:10.1007/bf00151270 (1981).

37 Wilde, S. A., Valley, J. W., Peck, W. H. & Graham, C. M. Evidence from detrital zircons for the existence of continental crust and oceans on the Earth 4.4 Gyr ago. Nature 409, 175-178, doi:10.1038/35051550 (2001).

38 Reinhard, C. T., Olson, S. L., Schwieterman, E. W. & Lyons, T. W. False Negatives for Remote Life Detection on Ocean-Bearing Planets: Lessons from the Early Earth. Astrobiology 17, 287-297, doi:10.1089/ast.2016.1598 (2017).

39 Schwieterman, E., Reinhard, C. T., Olson, S. & Lyons, T. W. The importance of UV capabilities for identifying inhaibted exoplanets with next generation space telescopes. arXiv 1801.02744 (2018).

40 Hayes, J. M. & Waldbauer, J. R. The carbon cycle and associated redox processes through time. Phil. Trans. R. Soc. B 361, 931-950, doi:10.1098/rstb.2006.1840 (2006).

41 Eguchi, J., Seales, J. & Dasgupta, R. Great Oxidation and Lomagundi events linked by deep cycling and enhanced degassing of carbon. Nat. Geosci. 13,

71-76, doi:10.1038/s41561-019-0492-6 (2020).

42 Evans, K. A. The redox budget of subduction zones. Earth-Science Reviews 113, 11-32, doi:https://doi.org/10.1016/j.earscirev.2012.03.003 (2012).

43 Kadoya, S., Catling, D. C., Nicklas, R. W., Puchtel, I. S. & Anbar, A. D. Mantle data imply a decline of oxidizable volcanic gases could have triggered the Great Oxidation. Nature Commun. 11, 2774, doi:10.1038/s41467-020-16493-1 (2020).

44 Lee, C.-T. A. et al. Two-step rise of atmospheric oxygen linked to the growth of continents. Nat. Geosci. 9, 417-424, doi:10.1038/ngeo2707 (2016).

45 Ozaki, K., Reinhard, C. T. & Tajika, E. A sluggish mid-Proterozoic biosphere and its effect on Earth's redox balance. Geobiology 17, 3-11, doi:10.1111/gbi.12317 (2019).

46 Ozaki, K., Tajika, E., Hong, P. K., Nakagawa, Y. & Reinhard, C. T. Effects of primitive photosynthesis on Earth's early climate system. Nat. Geosci. 11, 55-59, doi:10.1038/s41561-017-0031-2 (2018).

47 Kasting, J. F. Earth's early atmosphere. Science 259, 920-926, doi:10.1126/science.11536547 (1993).

48 Bergman, N. M., Lenton, T. M. & Watson, A. J. COPSE: A new model of biogeochemical cycling over Phanerozoic time. Am. J. Sci. 304, 397-437, doi:10.2475/ajs.304.5.397 (2004).

49 Laakso, T. A. & Schrag, D. P. Limitations on Limitation. Glob. Biogeochem. Cycles 32, 486-496, doi:doi:10.1002/2017GB005832 (2018).

50 Laakso, T. A. & Schrag, D. P. Methane in the Precambrian atmosphere. Earth Planet. Sci. Lett. 522, 48-54, doi:https://doi.org/10.1016/j.epsl.2019.06.022 (2019).

Corresponding author:
Correspondence to: Kazumi Ozaki, E-mail: kazumi.ozaki@sci.toho-u.ac.jp

Acknowledgements: The authors thank E. Tajika, Y. Sekine, S. Kadoya, Y. Watanabe, and E. Schwieterman for helpful discussions. K.O. acknowledges support from the NASA Postdoctoral Program at the NASA Astrobiology Program, administered by Universities Space Research Association under contact with NASA. This work was supported by JSPS KAKENHI Grant Number JP20K04066. C.T.R. acknowledges support from the NASA Astrobiology Institute (Grant 13-13NAI7_2-0027) and the NASA Nexus for Exoplanet System Science (NExSS) (Grant 80NSSC19KO461).

Author Contributions: K.O. and C.T.R. designed the study. K.O. constructed the model and performed experiments. K.O. and C.T.R. analysed the results and wrote the paper. All authors discussed and contributed intellectually to the interpretation of the results.

Competing interests: The authors declare no competing interests.

Methods

Model description. Our model is based on the Carbon Oxygen Phosphorus Sulphur Evolution (COPSE) model[12,48], the default version of which is described in full elsewhere[12,48]. The model has been extensively tested and validated against geologic records from the most recent ~500 million years of Earth's history and can predict the coupled histories and controls on atmospheric CO_2, O_2 and ocean composition (PO_4^{3-}, NO_3^-, SO_4^{2-}) on geologic timescales. The COPSE model was recently revised by ref.[51], but the version used here is based mainly on a previous version of the model described in ref.[12,15], because we have constructed the model with the aim of keeping the design as simple as possible. We do not anticipate our overarching conclusions to be altered by the differences. Our aim here is to produce a quantitative model that comprehensively encapsulates a range of key biogeochemical processes in oxic/anoxic biospheres and makes resulting predictions for the future lifespan of Earth's oxygenated atmosphere. Specifically, we made the following additions to the basic structure of the model: (1) metabolic CH_4 production/consumption processes in the ocean, (2) parameterized atmospheric photochemistry within the O_2-O_3-CH_4 system[24,25], (3) the radiative impact of CH_4 on global energy balance[26], (4) a dependence of marine phytoplankton growth rate on surface temperature[24] and marine inorganic carbon availability, (5) exchange of C, S, and Fe between the exogenic (ocean-atmosphere-crust) system and the mantle, and (6) a full redox (O_2) budget in the exogenic system.

Primary production and decomposition. In the COPSE model, the activity levels of terrestrial and marine ecosystems are evaluated separately. The global net primary production (NPP), J_{NPP} (in terms of organic carbon), is given by:

$$J_{\mathrm{NPP}} = J_{\mathrm{NPP}}^{\mathrm{ocn}} + J_{\mathrm{NPP}}^{\mathrm{land}}, \tag{1}$$

where J_{NPP}^{ocn} and J_{NPP}^{land} denote marine and terrestrial biospheric productivity, respectively. J_{NPP}^{ocn} is assessed as follows:

$$J_{\mathrm{NPP}}^{\mathrm{ocn}} = f_{\mathrm{n}} \cdot f_{T}^{\mathrm{ocn}} \cdot J_{\mathrm{NPP}}^{\mathrm{ocn},*}, \tag{2}$$

where * denotes the modern value of ~45 Gt C yr^{-1}, or 3750 Tmol C yr^{-1} (ref.[10]), and f_n and f_T^{ocn} denote the effect of nutrient availability and surface temperature on oceanic productivity, respectively. A Liebig's minimum law is adopted for f_n:

$$f_n = \frac{Minimum\left[r_{\mathrm{C/N}} N, r_{\mathrm{C/P}} P, M_{\mathrm{CO_2+HCO_3^-}} \right]}{r_{\mathrm{C/N}} N^*}, \tag{3}$$

1

where N, P, and $M_{CO2+HCO3-}$ denote reservoir sizes of seawater nitrate, phosphate and inorganic carbon (CO_{2aq} and HCO_3^-) available for phytoplankton growth, and $r_{C/P}$ (= 117) and $r_{N/P}$ (= 16) denote the "Redfield ratios" of photosynthetic biomass. In the original COPSE model the growth rate of marine phytoplankton is limited by the availability of nutrients (N or P). However, even in the modern ocean, CO_2-limitation can reduce growth rates among some phytoplankton taxa[52,53]. Given a secular decrease in atmospheric CO_2 levels (Fig. 2c), marine phytoplankton could be limited by the availability of dissolved inorganic carbon (CO_{2aq} and HCO_3^-) in the remote future. The dissolved concentrations of CO_{2aq} and HCO_3^- are calculated in the model by solving the

seawater carbonate system (see Supplementary Table 3). For the temperature response of marine phytoplankton growth, we adopt the following general function based on ref.[24];

$$f_{\mathrm{T}}^{\mathrm{ocn}}(T_{\mathrm{s}}) = \begin{cases} 0 & (T_{\mathrm{s}} < 273\ \mathrm{K}) \\ k\left\{1-\left(\dfrac{T_{\mathrm{opt}}-T_{\mathrm{s}}}{\Delta T_{\mathrm{opt}}}\right)^{2}\right\} & (273\ \mathrm{K} \le T_{\mathrm{s}} \le 301\ \mathrm{K}), \\ k\left[\left\{1-\left(\dfrac{T_{\mathrm{opt}}-T_{\mathrm{s}}}{\Delta T_{\mathrm{opt}}}\right)^{2}\right\}\cdot\exp\left(-\dfrac{\left|T_{\mathrm{s}}-T_{\mathrm{opt}}\right|^{3}}{T_{\mathrm{ref}}}\right)\right] & (T_{\mathrm{s}} \ge 301\ \mathrm{K}) \end{cases} \tag{4}$$

where k denotes a normalizing factor (= 1.2748), and T_{opt} and ΔT_{opt} are assumed to be 301 K and 301 K^3, respectively. The maximum temperature for phytoplankton growth is controlled by T_{ref}, whose uncertainty is explored by the statistical analysis (see below and Extended Data Figs. 1 and 3).

Almost all organic matter produced in the surface ocean is decomposed before burial. Fractions of organic matter decomposed by aerobic respiration (combined with denitrification/nitrification and microbial sulphate reduction/sulphide oxidation) and methanogenesis are expressed as follows:

$$f_{\mathrm{O_2}} = \frac{O}{O+K_{\mathrm{O_2}}}, \tag{5}$$

$$f_{\mathrm{CH_4}} = 1 - f_{\mathrm{O_2}}, \tag{6}$$

where O denotes the oxygen reservoir size in the combined ocean-atmosphere system and K_{O2} = 13.6×10^{18} mol. The total organic carbon decomposition rate is given by $J_{\mathrm{NPP}}^{\mathrm{ocn}} - J_{\mathrm{org}}^{\mathrm{b,ocn}} \equiv J_{\mathrm{org}}^{\mathrm{r,ocn}}$, where $J_{org}^{b,ocn}$ denotes the burial rate of organic carbon in marine sediments that is proportional to the square of the normalized primary production as in the original COPSE model[48]. The global methane generation rate via methanogenesis ($2\mathrm{CH_2O} \rightarrow \mathrm{CH_4} + \mathrm{CO_2}$) is given by $0.5 \times f_{\mathrm{CH_4}} \times J_{\mathrm{org}}^{\mathrm{r,ocn}}$. A fraction of this methane is consumed by aerobic/anaerobic methane oxidation processes (aerobic methanotrophy and AOM), given by:

$$\delta = \frac{O}{O+K_{\mathrm{O_2}}'}, \tag{7}$$

where K_{O2}' = 0.273×10^{18} mol (ref. [54]). Given the stoichiometric relationships, the net production rate of CH_4, CO_2, and O_2 in the ocean interior are given by:

$$J_{CH_4}^{ocn} = \frac{1}{2}(1-\delta)\cdot f_{CH_4}\cdot J_{org}^{r,ocn}, \quad (8)$$

$$J_{CO_2}^{ocn} = \left(f_{O_2} + \frac{1}{2}(1+\delta) f_{CH_4}\right)\cdot J_{org}^{r,ocn}, \quad (9)$$

$$J_{O_2}^{ocn} = J_{NPP}^{ocn} - \left(f_{O_2} + \delta f_{CH_4}\right)\cdot J_{org}^{r,ocn}. \quad (10)$$

For simplicity, the uncertainty associated with partitioning of CH_4 consumption between aerobic methanotrophy and AOM is accounted for implicitly by prescribing K_{O2}'.

The NPP of Earth's terrestrial biosphere is scaled by a factor V which represents global land biomass normalized by the modern value[48]:

$$J_{NPP}^{land} = V\cdot J_{NPP}^{land,*}, \quad (11)$$

where the NPP of the present terrestrial biosphere, $J_{NPP}^{land,*}$, is ~60 Gt Cyr^{-1}, or 5000 Tmol C yr^{-1} (ref.[10]), and V is calculated, as follows:

$$V = f_{UV}(O_2)\cdot f_P\cdot f_{fire}(O_2)\cdot V_{npp}(O_2, CO_2, T), \quad (12)$$

where V_{npp} denotes the effects of atmospheric O_2 and CO_2 concentrations and surface temperature on terrestrial biomass as in the original model (Extended Data Fig. 1a,b)[48], f_{fire} denotes the effect of the fire feedback[12,48], and f_P denotes a forcing factor representing selective-P weathering by vascular plant activity[12,15]. Our model introduces an additional factor, f_{UV}, in order to capture the effect of UV on the terrestrial biosphere as a function of atmospheric O_2 levels:

$$f_{UV}(O_2) = \tanh\left(\frac{pO_2(PAL)}{c_{UV}}\right), \quad (13)$$

where pO_2(PAL) denotes atmospheric O_2 levels in terms of PAL, and c_{UV} is treated as one of the model parameters explored during our stochastic analysis (see below). The minimum CO_2 concentration for the terrestrial plant activity is also treated as one of the uncertainties, because the ecological CO_2 threshold is not precisely known and its absolute value is likely to change with global mean temperature via its influence on photosynthesizer respiration rate[55,56].

The CH_4 flux from the terrestrial biosphere is assumed to be proportional to the burial rate of organic matter on land, as follows:

$$J_{CH_4}^{land} = \left(J_{org}^{b,land} / J_{org}^{b,land*}\right)\cdot f_T^{land}\cdot J_{CH_4}^{land,*}, \quad (14)$$

where f_T^{land} denotes the temperature effect on the CH_4 flux[57]:

$$f_T^{\text{land}} = a_{\text{CH}_4} \cdot \exp\left(b_{\text{CH}_4} \cdot T_{\text{C}} / T_{\text{C}}^*\right), \tag{15}$$

where T_C denotes the surface temperature in terms of °C. On the other hand, the net production rate of CH_4, CO_2, and O_2 in the terrestrial biosphere can be written, as follows:

$$J_{\text{CH}_4}^{\text{land}} = \frac{1}{2}(1-\delta) \cdot g_{\text{CH}_4} \cdot J^{\text{r,land}}, \tag{16}$$

$$J_{\text{CO}_2}^{\text{land}} = \left(g_{\text{O}_2} + \frac{1}{2}(1+\delta) g_{\text{CH}_4}\right) \cdot J^{\text{r,land}}, \tag{17}$$

$$J_{\text{O}_2}^{\text{land}} = J_{\text{NPP}}^{\text{land}} - \left(g_{\text{O}_2} + \delta g_{\text{CH}_4}\right) \cdot J^{\text{r,land}}, \tag{18}$$

where $J^{r,land}$ ($= J_{NPP}^{land} - J_{org}^{b,land}$) denotes the decomposition rate of organic matter in the terrestrial biosphere, and the fraction of methane oxidation is calculated by equation (7) above. A fraction of organic matter decomposed by methanogenesis, g_{CH4}, is determined from equations (14) and (16). Then g_{O2} is determined from $g_{\text{O}_2} = 1 - g_{\text{CH}_4}$.

Photochemistry. The revised model includes parameterized photochemistry that allows calculation of the concentrations of atmospheric O_2 and CH_4. We incorporate a scheme for parameterized O_2-O_3-CH_4 photochemistry based on the previous study of a 1-D photochemical model[24]. Specifically, the CH_4 oxidation rate k_{CH4ox} (in mol^{-1} y^{-1}) is expressed as a polynomial function of the reservoir sizes of O_2 and CH_4 (O and M)[25]:

$$\log k_{\text{CH}_4\text{ox}} = \alpha_0^j + \alpha_1^j \cdot \varphi_{\text{O}_2} + \alpha_2^j \cdot \varphi_{\text{O}_2}{}^2 + \alpha_3^j \cdot \varphi_{\text{O}_2}{}^3 + \alpha_4^j \cdot \varphi_{\text{O}_2}{}^4 + \alpha_5^j \cdot \varphi_{\text{O}_2}{}^5 + \alpha_6^j \cdot \varphi_{\text{O}_2}{}^6, \tag{19}$$

where α_i^j is fitting coefficients for a given atmospheric CH_4 levels and φ_{O2} is given by $\log pO_2$(bar) (Supplementary Table 4). The oxidation rate is evaluated based on Fig. 3 of ref. [24] showing the oxidation rate as a function of pO_2 and pCH_4. We took the relationship between k_{CH4ox} and pO_2 for pCH_4 of 10^{-6}, 10^{-5}, 10^{-4}, 10^{-3}, 2×10^{-3} bar, and k_{CH4ox} is calculated as a function of pO_2 and pCH_4 with a log-linear interpolation method.

For the atmospheres examined in this study, CH_4 and H_2O are the dominant hydrogen-bearing species in the stratosphere, allowing the hydrogen escape flux, J_{esc}, to be calculated as:

$$J_{\text{Hesc}} = f_{\text{esc}} \cdot f_{\text{T}}(\text{H}_2) = J_{\text{Hesc}}^{\text{H}_2\text{O}} + J_{\text{Hesc}}^{\text{CH}_4}, \tag{20}$$

where the proportional coefficient, f_{esc}, is 6.68×10^{15} mol yr^{-1} and $f_T(H_2)$ denotes the total hydrogen molecule mixing ratio:

$$f_{\text{T}}(\text{H}_2) = f\text{H}_2\text{O} + 2f\text{CH}_4. \tag{21}$$

Therefore, fluxes of hydrogen escape via CH_4 and H_2O are written in terms of the abundances in the stratosphere as:

$$J_{\mathrm{Hesc}}^{\mathrm{H_2O}} = f_{\mathrm{esc}} \cdot f\mathrm{H_2O}$$
$$J_{\mathrm{Hesc}}^{\mathrm{CH_4}} = 2 \cdot f_{\mathrm{esc}} \cdot f\mathrm{CH_4}. \tag{22}$$

We fit the empirical relationship between the stratospheric water vapour concentration and global average surface temperature obtained from a suite of 3-D GCM simulations of ref. [35] with a 3rd order polynomial in surface temperature:

$$\log_{10} f\mathrm{H_2O} = f_0 + f_1 T_K + f_2 {T_K}^2 + f_3 {T_K}^3, \tag{23}$$

where f_i denotes the fitting coefficients (f_0 = 198.34, f_1 = -1.6856, f_2 = 4.147×10^{-3}, and f_3 = -2.7947×10^{-6}) (Supplementary Fig. 2).

Subduction flux. Despite its crucial role in controlling the redox budget in the exogenic system, a process not typically represented in large-scale biogeochemical models is the subduction of redox sensitive elements (C, S, and Fe species) into the mantle. The exchange flux between Earth surface and the mantle influences not only the sizes of the surficial reservoirs but the oxygen balance of the atmosphere on the long timescales considered here. For the modern Earth the subduction flux of organic C is estimated at <0.2-0.7 Tmol O_2 equiv. yr^{-1} (ref. [40,42]), and that of sedimentary pyrite would also be small (<1 Tmol S yr^{-1})[42,58]. On the other hand, the rate of subduction of ferric iron could be 3 Tmol Fe yr^{-1} (0.75 Tmol O_2 equiv. yr^{-1})[40], or as high as 7 Tmol Fe yr^{-1} (1.75 Tmol O_2 equiv. yr^{-1})[59] to 19 Tmol Fe yr^{-1} (4.8 Tmol O_2 equiv. yr^{-1})[42]. However, there is a large uncertainty in the major oxidants (O_2 vs. SO_4^{2-}) for Fe^{2+} during aqueous oxidation of seafloor[60]. These redox-dependent subduction fluxes probably vary in intensity in response to changes in tectonic activity and oceanic redox state. In this study, the subduction fluxes of C, S, and Fe are parameterized as follows:

$$J_{\mathrm{org}}^{\mathrm{s}} = J_{\mathrm{org}}^{\mathrm{s,*}} \cdot \left(\frac{J_{\mathrm{org}}^{\mathrm{b}}}{J_{\mathrm{org}}^{\mathrm{b,*}}} \right) \cdot f_{\mathrm{G}}, \tag{24}$$

$$J_{\mathrm{carb}}^{\mathrm{s}} = J_{\mathrm{carb}}^{\mathrm{s,*}} \cdot \left(\frac{J_{\mathrm{carb}}^{\mathrm{b}}}{J_{\mathrm{carb}}^{\mathrm{b,*}}} \right) \cdot f_{\mathrm{G}} \tag{25}$$

$$J_{\mathrm{py}}^{\mathrm{s}} = J_{\mathrm{py}}^{\mathrm{s,*}} \cdot \left(\frac{J_{\mathrm{py}}^{\mathrm{b}}}{J_{\mathrm{py}}^{\mathrm{b,*}}} \right) \cdot f_{\mathrm{G}} \tag{26}$$

$$J_{\mathrm{Fe\text{-}ox}}^{\mathrm{s}} = J_{\mathrm{Fe\text{-}ox}}^{\mathrm{s,*}} \cdot \left(\frac{1 - DOA}{1 - DOA^*} \right) \cdot f_{\mathrm{G}} \tag{27}$$

where * denotes a reference value, which is treated as a free parameter. The rate of subduction is scaled to the tectonic activity represented by a forcing f_G (D in the original COPSE model). The subduction fluxes of organic carbon and carbonate carbon are also proportional to their burial

fluxes. We also assume that the subduction flux of Fe-oxides is a function of the degree of anoxia (DOA) which represents oceanic anoxicity. The rate of subduction of ferric iron is thought to be sensitive to the redox landscape of the global ocean (e.g., sulfidic or Fe-rich anoxia), but this is outside the scope of the present work. Even if subduction of iron oxides is assumed to continue in an anoxic, Fe-rich ocean, this would not change our overarching conclusion that the future lifespan of the oxygenated atmosphere is less than 1.5 Gyr because the subduction of ferric iron represents the loss of oxidizing power from the surface system. Given the large uncertainty in the magnitude of subduction fluxes, we explore a wide range of reference values in our stochastic analysis (Extended Data Fig. 3).

Global O_2 budget. In this study, redox balance in the model is tracked in units scaled to the oxidizing power of O_2. The model explicitly accounts for fluxes of oxidants and reductants into and out of the surface system (Supplementary Fig. 3). The global redox budget (GRB) for the ocean-atmosphere system (OAS) is written as follows:

$$GRB_{\mathrm{OAS}} = 0.5J_{\mathrm{Hesc}} + \left(J^{\mathrm{b,ocn}}_{\mathrm{org}} + J^{\mathrm{b,t}}_{\mathrm{org}} - J^{\mathrm{w}}_{\mathrm{org}} - J^{\mathrm{m}}_{\mathrm{org}}\right) + \left(2J^{\mathrm{b}}_{\mathrm{py}} - 2J^{\mathrm{w}}_{\mathrm{py}}\right) - 2J^{\mathrm{d}}_{\mathrm{H_2S}} - J^{\mathrm{d}}_{\mathrm{red}} - 0.25J^{\mathrm{s}}_{\mathrm{Fe\text{-}ox}} \quad (28)$$

where J_{Hesc} denotes the irreversible hydrogen escape to space, and second and third terms represent the influence of organic C and pyrite S subcycles on the GRB. $J_{H2S}{}^{d}$ and $J_{red}{}^{d}$ are the mantle degassing of H_2S and other reducing gases (e.g., H_2). $J_{Fe\text{-}Ox}{}^{s}$ is the subduction flux of ferrous iron. In this study, we also revised the baseline COPSE model to capture the O_2 budget in the exogenic (ocean-atmosphere-crust) system on geological timescales, according to:

$$GRB_{\mathrm{exo}} = 0.5J_{\mathrm{Hesc}} + J^{\mathrm{s}}_{\mathrm{org}} + 2J^{\mathrm{s}}_{\mathrm{py}} - 0.25J^{\mathrm{s}}_{\mathrm{Fe\text{-}ox}} - 2J^{\mathrm{d}}_{\mathrm{H_2S}} - J^{\mathrm{d}}_{\mathrm{red}}. \quad (29)$$

The primary sink of reducing power from the exogenic system is the irreversible escape of hydrogen to space (J_{Hesc}) and the subduction of organic C and pyrite S to the mantle ($J_{org}{}^{s}$ and $J_{py}{}^{s}$), while the primary source of reducing power is outgassing of reduced gases from the Earth's interior ($J_{H2S}{}^{d}$ and $J_{red}{}^{d}$). The subduction of ferric iron ($J_{Fe\text{-}ox}{}^{s}$) is also a loss of oxidizing power (i.e., source of reducing power). The net input flux of reducing power from the mantle to the exogenic system is defined as:

$$\Phi(\mathrm{Red}) = -J^{\mathrm{s}}_{\mathrm{org}} - 2J^{\mathrm{s}}_{\mathrm{py}} + 0.25J^{\mathrm{s}}_{\mathrm{Fe\text{-}ox}} + 2J^{\mathrm{d}}_{\mathrm{H_2S}} + J^{\mathrm{d}}_{\mathrm{red}}. \quad (30)$$

In Fig. 3b of the main text, we assess the impact of long-term Φ(Red) on the future lifespan of oxygenated atmosphere. To do this, we average Φ (Red) over the future lifespan:

$$\overline{\Phi_i(\mathrm{Red})} = \frac{\int_0^{\tau_i} \Phi(\mathrm{Red})dt}{\tau_i}, \quad (31)$$

where τ_i denotes the future lifespan for the different values of O_2 threshold i (in PAL). Existing empirical estimates of the mantle degassing of reducing gases via submarine volcanism, 0.7±0.3 Tmol O_2 equiv. yr^{-1} (ref. [60]), the limited O_2 consumption through seafloor Fe^{2+} oxidation 0.14 Tmol O_2 equiv. yr^{-1} (ref. [60]), and the subduction flux of organic C of <0.2-0.7 Tmol O_2 equiv. yr-

[1], yield a present net input flux of reducing power from the mantle to the surface system, □(Red)*, of >-0.16 Tmol O_2 equiv. yr^{-1}. A resampling analysis of Φ(Red)* from our successful model simulations predicts a slightly lower value of -0.24±0.27 Tmol O_2 equiv. yr^{-1} (Supplementary Fig. 4).

Climate model. Global mean surface temperature T_s (in K) is estimated with a zero-dimensional energy balance model (0-D EBM) in which the absorption of solar radiation is balanced by the heat loss by outgoing longwave (i.e., infrared) radiation (OLR) to space (J_{OLR}):

$$(1\text{-}\alpha)\cdot\frac{S_{\odot}}{4} = J_{\mathrm{OLR}} - RF_{\mathrm{CH_4}}, \tag{32}$$

where α and $S_{\odot}$ denote the top-of-atmosphere (TOA) albedo and the value of the solar constant at the time under consideration, respectively. For J_{OLR} and α, we adopted the parametric expressions proposed by ref.[61], with the following variables: p = pCO_2 (in bar); $\phi = \ln(p/3.3\times10^{-4})$; μ = cos(z), where z is the zenith angle; and surface albedo α_s. α_s is written as a function of T_s:

$$\alpha_s = \begin{cases} \alpha_{00} & (T_0 \le T_s) \\ \alpha_{\mathrm{ice}} - (\alpha_{\mathrm{ice}} - \alpha_{00})\cdot\dfrac{(T_s - T_{\mathrm{ice}})^2}{(T_s - T_{\mathrm{ice}})^2} & (T_{\mathrm{ice}} \le T_s \le T_0) \\ \alpha_{\mathrm{ice}} & (T_s \le T_{\mathrm{ice}}) \end{cases}, \tag{33}$$

where it is assumed that Earth is globally ice-covered for $T_s < T_{ice}$ (= 263 K) with an albedo $□_{ice}$ (= 0.65), and that Earth is characterized by a relatively low albedo α_0 (= 0.35) for $T_s > T_0$ (= 273K). For $T_{ice} < T_s < T_0$, the albedo is interpolated with a quadratic interpolation method[62]. RF_{CH4} represents the radiative forcing by methane, which is quantified based on ref.[26]. Recent 1-D modelling results suggest that relatively small increases in solar luminosity could conceivably trigger a runaway greenhouse on Earth[63,64]. However, 3-D climate models indicate that Earth's climate is likely to be somewhat more stable than this as a consequence of expansion of unsaturated regions in the upper atmosphere attendant to changes in Hadley circulation that occur at higher solar fluxes[23,65]. Given the quantitative consistency between the above 0-D EBM and recent 3-D climate models[35] (Supplementary Fig. 1), we consider our utilization of 0-D EBM a defensible approximation of planetary climate for implementation on 10^6-10^9-year timescales. Nevertheless, it is important to point out that future projections of Earth system behavior will likely be modulated by uncertain cloud feedbacks and continental configurations. As a result, in our MC analysis we explore uncertainties in OLR and TOA (Extended Data Fig. 3).

Stochastic analysis. The computational efficiency of the model enables us to examine the future lifespan of the oxygenated atmosphere via a stochastic analysis, in which we randomly sample from a prior distribution for poorly constrained parameters and quantify whole-model uncertainty (Extended Data Fig. 3). We draw poorly constrained initial values for crustal C and S reservoir sizes at 600 Ma (million years ago) over a wide range of values. We also vary the reference values

of fluxes between the exogenic system and the mantle (subduction and mantle degassing) to capture uncertainties in model parameterisation. After running the model forwards in time until the present, we only sample model runs that allow for acceptable atmospheric composition (pO_2 = 21±1% and pCO_2 = 300±150 ppmv), global surface temperature (288±2K) and seawater sulphate (SO_4^{2-}) levels (SO_4^{2-} = 25±15 mM). The model runs that fail to obtain reasonable values have been abandoned. For our default stochastic analysis, we performed nearly 400,000 simulations to span the whole parameter space, and the resultant successful runs were n = 4,787 which were continued to be run for estimating the future lifespan of the oxygenated atmosphere.

For the future evolution of the degassing factor (f_G) and erosion factor (f_R; U in the original model), we assumed following functions:

$$f_{\mathrm{G}} = \left(1 + a_{\mathrm{G}} + a_{\mathrm{G}} \sin\left(2\pi \frac{t - \tau_{\mathrm{G}}/4}{\tau_{\mathrm{G}}}\right)\right) \cdot \left(\left(1 + \frac{t}{4500}\right)^{-n}\right)^{m}, \tag{34}$$

$$f_{\mathrm{R}} = \left(1 + a_{\mathrm{R}} \sin\left(2\pi \frac{t - \tau_{\mathrm{R}}}{\tau_{\mathrm{R}}}\right)\right) \cdot \left(\left(1 + \frac{t}{4500}\right)^{-n}\right)^{m}, \tag{35}$$

where the first term on the right-hand side denotes the periodic changes with an amplitude a and a period of τ (in Myr), and the second term represents the secular decrease in the activity of tectonics[66]. These relationships have been adopted for examining to the geological past, and we consider that this assumption is a reasonable first-order approximation as there is no a priori reason for thinking that this style of decay will not continue into Earth's far future. Nevertheless, we also emphasize that this is very under-studied and it is possible that non-linearity in tectonic regime will be important to consider for Earth and other habitable rocky planets in future work.

We draw model parameters from wide distributions that represent the uncertainty in their values (Extended Data Fig. 3). For example, the uncertainty in the biological responses is assessed by changing biological parameters, such as FERT. The strength of terrestrial weathering feedback is also a topic of debate[67-69], and we explore its uncertainty by changing the apparent activation energy (ACT) and a runoff factor (RUNsil)[70]. The amplification of terrestrial weatherability by land plants is also an important uncertainty[71,72], which we explore here by changing LIFE[70]. To account for the uncertainty in the value of c_{UV}, we draw it from a log-uniform distribution between $10^{-2.5}$ PAL and $10^{-1.5}$ PAL (Extended Data Fig. 1c). At the higher end of this range, terrestrial plant activity is suppressed when atmospheric O_2 is <10% PAL. At the lower end, the threshold is lowered to ~1%PAL. We consider these two end-member cases to cover the full range of uncertainty of UV impacts on the terrestrial ecosystems. We also explore uncertainty in the strength of redox-dependent P recycling in marine sediments by changing C_{org}/P_{org} ratios for anoxic sediments.

The sampling procedure is run for long enough to obtain stationary distributions for posterior probability densities. However, it is possible that our model predictions may underestimate the

inherent variability in the future Earth's evolution. For instance, the possibility of random catastrophe, such as the asteroid impacts, could also introduce additional uncertainty in the estimate of future lifespan of Earth's oxygenated atmosphere. We also note that the uncertainty in the longevity of human impacts on Earth's future environment is beyond the scope of this study.

Data availability. The numerical data for Figure 3 in the main text and Extended Data Figures 4 and 5 are presented in the Source data. The big data obtained by the statistical analysis is available to download at https://doi.org/10.6084/m9.figshare.13487487.v1.

Code availability. Our Fortran source code is available at https://github.com/kazumi-ozaki/lifespan.

References

51 Lenton, T. M., Daines, S. J. & Mills, B. J. W. COPSE reloaded: An improved model of biogeochemical cycling over Phanerozoic time. Earth-Science Reviews 178, 1-28, doi:https://doi.org/10.1016/j.earscirev.2017.12.004 (2018).

52 Hein, M. & Sand-Jensen, K. CO_2 increases oceanic primary production. Nature 388, 526-527, doi:10.1038/41457 (1997).

53 Riebesell, U., Wolf-Gladrow, D. A. & Smetacek, V. Carbon dioxide limitation of marine phytoplankton growth rates. Nature 361, 249-251, doi:10.1038/361249a0 (1993).

54 Goldblatt, C., Lenton, T. M. & Watson, A. J. Bistability of atmospheric oxygen and the Great Oxidation. Nature 443, 683-686, doi:http://www.nature.com/nature/journal/v443/n7112/suppinfo/nature05169_S1.html (2006).

55 Galbraith, E. D. & Eggleston, S. A lower limit to atmospheric CO_2 concentrations over the past 800,000 years. Nat. Geosci. 10, 295-298, doi:10.1038/ngeo2914 (2017).

56 Pagani, M., Caldeira, K., Berner, R. & Beerling, D. J. The role of terrestrial plants in limiting atmospheric CO_2 decline over the past 24 million years. Nature 460, 85-88, doi:10.1038/nature08133 (2009).

57 Beerling, D., Berner, R. A., Mackenzie, F. T., Harfoot, M. B. & Pyle, J. A. Methane and the CH4 related greenhouse effect over the past 400 million years. Am. J. Sci. 309, 97-113, doi:10.2475/02.2009.01 (2009).

58 Canfield, D. E. The evolution of the Earth surface sulfur reservoir. Am. J. Sci. 304, 839-861, doi:10.2475/ajs.304.10.839 (2004).

59 Lécuyer, C. & Ricard, Y. Long-term fluxes and budget of ferric iron: implication for the redox states of the Earth's mantle and atmosphere. Earth Planet. Sci. Lett. 165, 197-211, doi:https://doi.org/10.1016/S0012-821X(98)00267-2 (1999).

60 Catling, D. C. & Kasting, J. F. Atmospheric Evolution on Inhabited and Lifeless Worlds. (Cambridge University Press, 2017).

61 Williams, D. M. & Kasting, J. F. Habitable Planets with High Obliquities. Icarus 129, 254-267, doi:http://dx.doi.org/10.1006/icar.1997.5759 (1997).

62 Pierrehumbert, R. T., Abbot, D. S., Voigt, A. & Koll, D. Climate of the Neoproterozoic. Annu. Rev. Earth Planet. Sci. 39, 417-460, doi:10.1146/annurev-earth-040809-152447 (2011).

63 Goldblatt, C., Robinson, T. D., Zahnle, K. J. & Crisp, D. Low simulated radiation limit for runaway greenhouse climates. Nat. Geosci. 6, 661-667, doi:10.1038/ngeo1892 (2013).
64 Kopparapu, R. K. et al. Habitable Zones around Main-sequence Stars: New Estimates. Astrophys. J. 765, 131 (2013).
65 Abe, Y., Abe-Ouchi, A., Sleep, N. H. & Zahnle, K. J. Habitable zone limits for dry planets. Astrobiology 11, 443-460, doi:10.1089/ast.2010.0545 (2011).
66 Krissansen-Totton, J., Arney, G. N. & Catling, D. C. Constraining the climate and ocean pH of the early Earth with a geological carbon cycle model. Proc. Natl Acad. Sci. USA 115, 4105-4110, doi:10.1073/pnas.1721296115 (2018).
67 Krissansen-Totton, J. & Catling, D. C. Constraining climate sensitivity and continental versus seafloor weathering using an inverse geological carbon cycle model. Nature Commun. 8, 15423, doi:10.1038/ncomms15423 (2017).
68 Graham, R. J. & Pierrehumbert, R. Thermodynamic and Energetic Limits on Continental Silicate Weathering Strongly Impact the Climate and Habitability of Wet, Rocky Worlds. Astrophys. J. 896, 115, doi:10.3847/1538-4357/ab9362 (2020).
69 Winnick, M. J. & Maher, K. Relationships between CO_2, thermodynamic limits on silicate weathering, and the strength of the silicate weathering feedback. Earth Planet. Sci. Lett. 485, 111-120, doi:https://doi.org/10.1016/j.epsl.2018.01.005 (2018).
70 Royer, D. L. Atmospheric CO_2 and O_2 During the Phanerozoic: Tools, Patterns, and Impacts. 251-267, doi:10.1016/b978-0-08-095975-7.01311-5 (2014).
71 Ibarra, D. E. et al. Modeling the consequences of land plant evolution on silicate weathering. Am. J. Sci. 319, 1-43, doi:10.2475/01.2019.01 (2019).
72 Moulton, K. L. & Berner, R. A. Quantification of the effect of plants on weathering: Studies in Iceland. Geology 26, 895-898, doi:10.1130/0091-7613(1998)026<0895:qoteop>2.3.co;2 (1998).